

Acoustic levitation of super-wavelength elastic films using ultrasound phased arrays

Cite as: Appl. Phys. Lett. **126**, 052204 (2025); doi: 10.1063/5.0247416

Submitted: 7 November 2024 · Accepted: 27 January 2025 ·

Published Online: 5 February 2025



View Online



Export Citation



CrossMark

Gakuto Arakawa,^{a)} Shun Suzuki,^{b)} Takaaki Kamigaki,^{c)} Yasutoshi Makino,^{d)} and Hiroyuki Shinoda^{e)}

AFFILIATIONS

Graduate School of Frontier Sciences, The University of Tokyo, 5-1-5 Kashiwa-no-ha, Kashiwa City, Chiba 277-8561, Japan

^{a)}Author to whom correspondence should be addressed: arakawa@hapis.k.u-tokyo.ac.jp

^{b)}Electronic mail: suzuki@hapis.k.u-tokyo.ac.jp

^{c)}Electronic mail: kamigaki@hapis.k.u-tokyo.ac.jp

^{d)}Electronic mail: yasutoshi_makino@k.u-tokyo.ac.jp

^{e)}Electronic mail: hiroyuki_shinoda@k.u-tokyo.ac.jp

ABSTRACT

We present a method for levitating films with a surface size larger than the wavelength using airborne ultrasound phased arrays. A typical example is a polyimide film with a side length of 40–50 mm and a thickness of 5 μm (aspect ratio: $8–10 \times 10^3$). We verified our method by measuring the height, horizontal position, and vibration of the levitating film. The results show that the film levitates at the height of the original standing wave node and at discrete horizontal positions approximately every transducer interval. The levitated film vibrates at the same frequency as the ultrasonic transducer and cannot be regarded as rigid against ultrasonic waves. Different film materials and thicknesses were examined, including metal foils and wood papers. In this study, the maximum surface density of the films that levitated was $3.5 \times 10^{-2} \text{ mg/mm}^2$. Therefore, the proposed method can be used to hold film samples in the air for observation or as an aerial screen.

© 2025 Author(s). All article content, except where otherwise noted, is licensed under a Creative Commons Attribution-NonCommercial-NoDerivs 4.0 International (CC BY-NC-ND) license (<https://creativecommons.org/licenses/by-nc-nd/4.0/>). <https://doi.org/10.1063/5.0247416>

Acoustic levitation is a method for levitating objects using acoustic radiation force. Objects can be levitated in the air at a distance of more than a wavelength from the sound source by forming standing^{1–8} or traveling^{8–10} waves of airborne ultrasound. Solids and liquids^{11,12} can be levitated if their acoustic impedance is sufficiently different from that of the air. Applications are being developed in biochemistry,^{13,14} robotics,¹⁵ and human interfaces.^{4,16,17} Because the acoustic radiation force can be considered an area force at boundary surfaces where ultrasonic waves mostly reflect, such as between air and solids,¹⁸ levitation methods using airborne ultrasounds should be validated according to the size and shape of the object being levitated. For spherical objects, levitation methods have been proposed for sufficiently small,^{1,9} comparable (Mie size),¹⁰ and larger sizes,⁸ relative to the wavelength. For non-spherical beads, radiation forces and torques were theoretically studied,¹⁹ and rotation suppression was achieved for small to Mie objects.^{2,3} Other examples include the levitation of rod-shaped objects^{4,5} and an object with a curved surface.²⁰ For thin films, a 25–50 μm -thick film with a diameter smaller than the wavelength was levitated and rotated.^{6,7} This film levitation has potential applications in the protein crystallography.²¹

In this study, we present a method for levitating films that are approximately 1–25 μm thick and over 40 mm wide using airborne ultrasound phased arrays (AUPAs). Our method can be implemented using only quasi-plane waves and does not require complex phase calculations. Films can be levitated for more than 30 s and can be stabilized for more than 1 min, depending on their materials and thicknesses. The ultrasound frequency was 40 kHz, which means that the wavelength was $\lambda \approx 8.5 \text{ mm}$ at room temperature. The width of the film L used in this study was larger than the wavelength ($L > 4\lambda$). Moreover, the fundamental characteristics of our method, such as the levitation position, film vibration, and film materials, are evaluated.

We describe a system for levitating thin films with edges larger than the wavelength. In our method, the AUPAs are placed vertically, opposite to each other, as shown in Fig. 1 (Multimedia view). The AUPAs are aligned so that each upper transducer is directly above the lower transducer. In the experiments, we used AUTD3 units,²² which can be synchronized within 0.1 μs as the AUPAs. A single AUTD3 unit has 249 transducers (T4010A1, Nippon Ceramic Co., Ltd.) and is driven at a 24 V_{p-p} (peak to peak) voltage. Each transducer features a diameter of 10 mm and 10.16 mm spacing

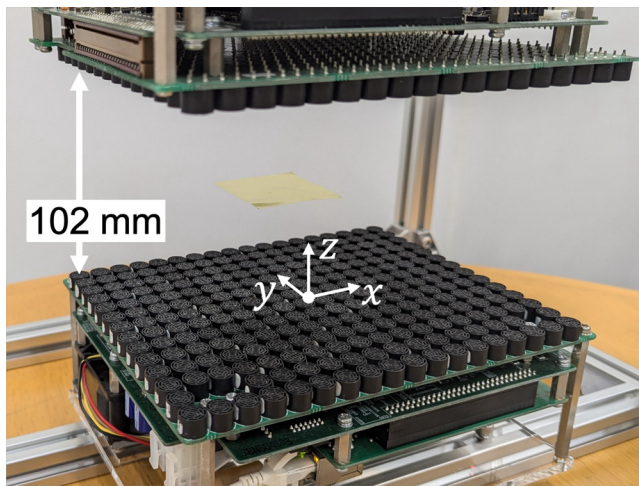


FIG. 1. Example of film levitation using our method. A yellow polyimide film, 40 mm × 40 mm and 5 μm thick, is levitating. Multimedia available online.

alignment.²² The distance between the upper and lower AUPAs D_{AUPA} was set to 102 mm ($= 12\lambda$).

Each transducer of the lower/upper AUPA is fixed to a common phase $\phi_{\text{lwr}}/\phi_{\text{upr}}$ so that quasi-plane waves are emitted parallel to each AUPA surface. The phase difference $\Delta\phi = \phi_{\text{lwr}} - \phi_{\text{upr}}$ can be considered in the range $0 \leq \Delta\phi \leq \pi$. The acoustic pressure at the position \mathbf{r} in the standing wave can be written as

$$\begin{aligned} P(\mathbf{r}) &= P_{\text{lwr}}(\mathbf{r}) + P_{\text{upr}}(\mathbf{r}) \\ &= \sum_i A \left(\frac{e^{j(k|\mathbf{r} - \mathbf{r}_{\text{lwr}}^i| + \phi_{\text{lwr}})}}{|\mathbf{r} - \mathbf{r}_{\text{lwr}}^i|} + \frac{e^{j(k|\mathbf{r} - \mathbf{r}_{\text{upr}}^i| + \phi_{\text{upr}})}}{|\mathbf{r} - \mathbf{r}_{\text{upr}}^i|} \right) e^{-j\omega t}, \quad (1) \end{aligned}$$

where A is the acoustic pressure amplitude for all transducers (unified at their maximum), j is the imaginary unit, k is the wavenumber, t is the time, and $\mathbf{r}_{\text{lwr}}^i/\mathbf{r}_{\text{upr}}^i$ is the position of the i th transducer of the lower/upper AUPA. The origin is the center of the lower AUPA surface, and the x -, y -, and z -axes are the longitudinal, shortitudinal, and normal directions of the AUPA, respectively. For example, the acoustic pressure distributions of the standing wave when $\Delta\phi = 0$, and π , are shown in Fig. 2. The distributions are calculated assuming that each transducer is a non-directional point source. Note that no film is inserted into the acoustic field in Fig. 2. At $z = D_{\text{AUPA}}/2$, the ultrasonic waves strengthen each other when $\Delta\phi = 0$, whereas they cancel each other when $\Delta\phi = \pi$. In the former case, weakening occurs at approximately $z = D_{\text{AUPA}}/2 \pm \lambda/4$, and the acoustic pressure becomes low. A periodicity dependent on the transducer spacing is observed in the x and y directions in the standing wave because the AUPAs do not form a uniform plane wave, even if the transducers are in phase.

When a piece of film is inserted horizontally into the standing wave, it levitates at specific positions without rotation. In the experiment, film pieces of known dimensions were used to measure the levitation height and horizontal position. Note that the levitated film was static-free.

We measured the film levitation height using two AUTD3 units and a horizontal green laser source, as shown in Fig. 3(a). In this study, 5 μm-thick polyimide films with three sizes were used: 40 mm × 40 mm,

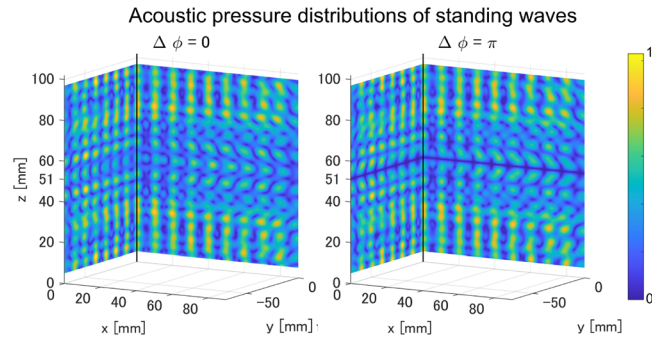


FIG. 2. Simulated acoustic pressure distributions (absolute value) of standing waves without a film using Eq. (1). Normalized acoustic pressure is shown. Periodicity is observed in each axis direction because transducer arrays are the sound source.

50 mm × 40, and 50 mm × 50 mm. Two conditions, $\Delta\phi = 0, \pi$, were used for the phase difference of the AUPAs. The thin film was transparent and experimentally found to be not completely planar. Thus, laser light with a width of approximately 1 mm was reflected from the film surfaces. The reflected light on the film can be quantified as the number of green pixels observed when capturing it with a camera. Thus, the larger number of green pixels was regarded as the levitation height being close to the laser height. The height of the horizontal laser light H_{lsr} was varied at 1 mm intervals with respect to an unknown film levitation height H_{flm} . Levitating films were captured with a camera (1920 px × 1080 px, 60 fps) for 10 s, and the time-averaged number of green pixels on the film surface α was counted [Fig. 3(b)].

The value of α for each film size is plotted on the vertical axis as H_{lsr} in Fig. 4. A larger value of α indicates that H_{flm} and H_{lsr} are close. These results show that the levitation height depends on the phase difference $\Delta\phi$ and is independent of the film size. When $\Delta\phi = \pi$, the levitation height was 51 mm, which means that $H_{\text{flm}} = D_{\text{AUPA}}/2$. When $\Delta\phi = 0$, the levitation heights were approximately 49 and 53 mm. Because $\lambda/4 \approx 2.1$ mm, the height can be regarded as $H_{\text{flm}} = D_{\text{AUPA}}/2 \pm \lambda/4$.

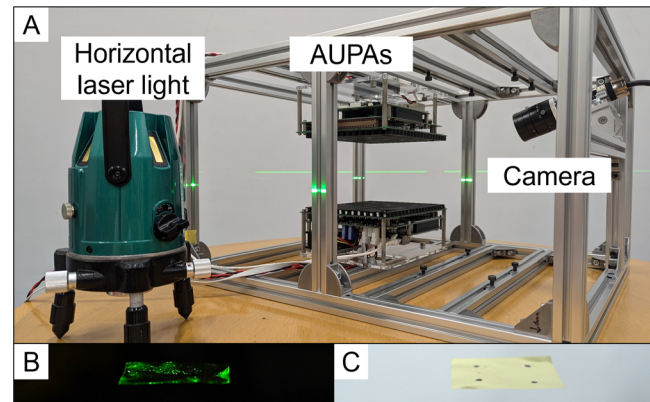


FIG. 3. (a) Setup for measuring the film's levitation position. (b) The film is exposed to a horizontal laser light to measure the levitation height. (c) The film is marked with four dot markers to measure the horizontal position.

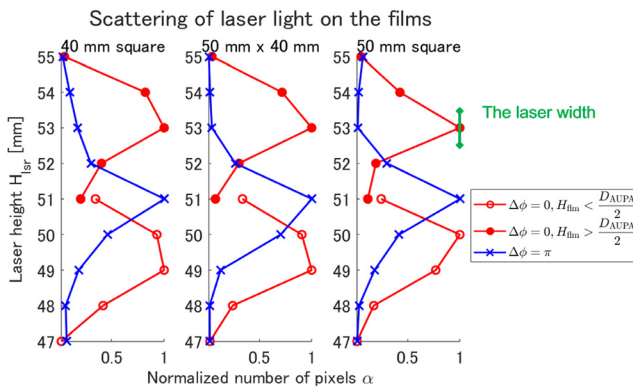


FIG. 4. Measured levitation heights of the films. The stronger the scattering of the laser light on the film, the larger the value of α . That is, H_{ls} with $\alpha=1$ represents the levitation height under each condition. Each height has an error of ± 0.5 mm due to the width of the laser. Two levitation heights with $\Delta\phi=0$ were found; therefore, the measurements were taken separately (red lines).

We then measured the horizontal levitation positions of the film using a high-speed camera ($1920 \text{ px} \times 1200 \text{ px}$). Only $\Delta\phi=\pi$ was used for the phase difference, and the film was captured for 5 s at 100 fps after confirming that the film was levitating at $z=51 \text{ mm}$ using a horizontal laser light. As with the height measurements, three sizes of polyimide film were examined. We drew black dots on the surface of each film to measure its posture simultaneously [Fig. 3(c)]. The xy -coordinates of the film center were estimated using the dots captured by the camera.

Figure 5 shows the time-averaged xy -coordinates of the film center. The levitating film exhibited minute horizontal vibrations in the range of 1–2 mm, as shown in the enlarged figure. Note that only the representative cases that were measured in this experiment are shown.

That is, some of the possible positions were not covered. Because the levitation positions were distributed in grid-like patterns, straight lines were drawn as a guide for the square films. The levitation positions away from the center of the aperture, such as $x=37.2-42.3 \text{ mm}$, also follow these grid-like patterns. The $50 \text{ mm} \times 40 \text{ mm}$ film levitates near the intersections of the different colored lines. That is, the xy -coordinates of the levitation position depend on the lengths of the edges in each direction. The average distance between these grid points for all sizes was 10.5 mm in the x direction and 10.9 mm in the y direction.

The four black dots on the film were placed at the vertices of a rectangle whose sides were parallel to the sides of the film. As shown in the lower right panel of Fig. 5, θ is the angle between the $x=0$ plane and the line connecting the black dots near the y -axis (bottom left and top left dots) on the film. The figure shows the time variation of θ for the case of a 40 mm square film. The time average value of θ was -0.1 deg , which means that the film was stable in an orientation in which its edge directions coincided with the directions of the transducer alignment.

The vibrations of the levitating film were measured using a laser Doppler vibrometer (LV-1800, ONO SOKKI) to determine whether the film was acoustically rigid. In this measurement, four AUTD3 units were set up, as shown in Fig. 6, such that the laser beam of the vibrometer passed vertically through a 10 mm gap. A $5 \mu\text{m}$ -thick polyimide film that was $50 \text{ mm} \times 50 \text{ mm}$ in size was levitated at $z=51 \text{ mm}$ with $\Delta\phi=\pi$, and the vibration of the film was measured for 1 s at a sampling frequency of 98.1 kHz .

Figure 7 shows the frequency distribution of the measurement results. The frequency peak at 40.004 kHz corresponds to the ultrasonic frequency emitted from the AUTD3 units, as measured by the microphone. The vibration velocity amplitude at 40.004 kHz was 0.41 m/s . Therefore, the displacement amplitude was estimated to be $0.41/(2\pi \times 40,004) = 1.6 \mu\text{m}$. These results indicate that the film is not acoustically rigid but does vibrate at the same frequency as the

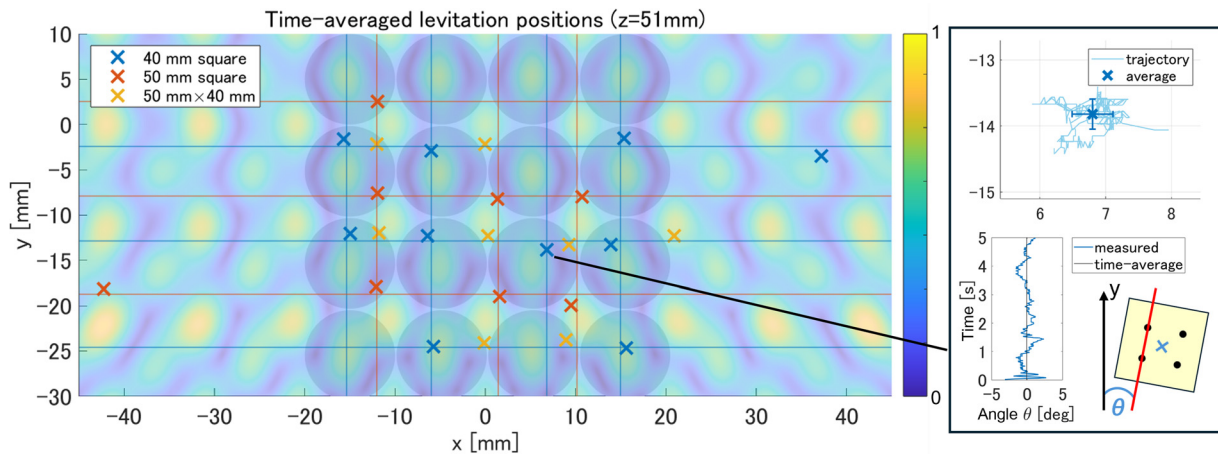


FIG. 5. Time-averaged horizontal positions of the centers of the levitating films for 5 s. For the square films, the expected grid was drawn from the measurements. The positions of the transducers are indicated by gray circles. A color map overlays the incident wave from the lower AUPA, illustrating the normalized sound pressure distribution. The incident wave from the upper AUPA and scattering on the film are ignored. For the case of a 40 mm square with a time-averaged center position of $(6.80 \text{ mm}, -13.8 \text{ mm})$, the film center trajectory with error bar (standard deviations in the x and y directions, respectively) is shown in the upper right panel, and the time variation of angle θ with the y -axis is shown in the lower right panel.

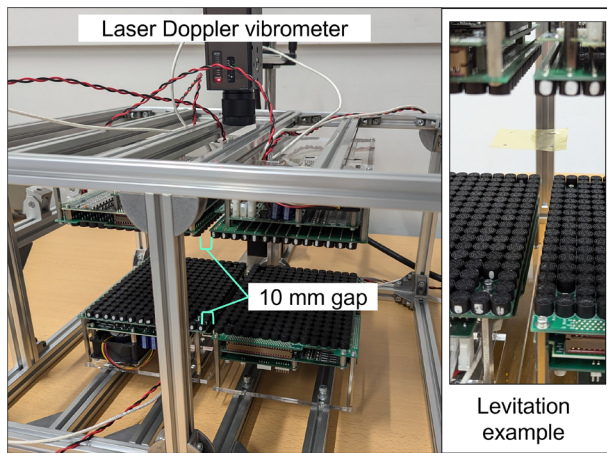


FIG. 6. Setup for measuring film vibration using a laser Doppler vibrometer. Four AUTD3 units were fixed with a 10 mm gap. The film was levitated to a position visible through the gap and measured by directing the laser beam vertically.

sound source and re-radiates the ultrasonic waves. Vibrations above 49.05 kHz were not examined because the sampling frequency was 98.1 kHz.

Films of different materials and thicknesses were tested to evaluate whether they could be levitated. The films in **Table I** were prepared in sizes of 40 mm × 40 mm and levitated at $z = 51$ mm with $\Delta\phi = \pi$. A setup with two AUTD3 units was used, as shown in **Fig. 3**. We judged the films to be levitable if they did not rotate, translate, or deform for more than 30 s, except for microvibrations, similar to the 5 μm polyimide film. Five retries were allowed for each film because the initial position and posture had to be adjusted manually. All films determined not to be levitable were either not lifted into the air or not stable in a horizontal position, from the beginning. Among the levitated films, the 25 μm polyester film had the largest surface density $3.5 \times 10^{-2} \text{ mg/mm}^2$. Vibrations were also measured for a 4.4 μm aramid film and a 5 μm polyester film, using the method shown in **Fig. 6**.

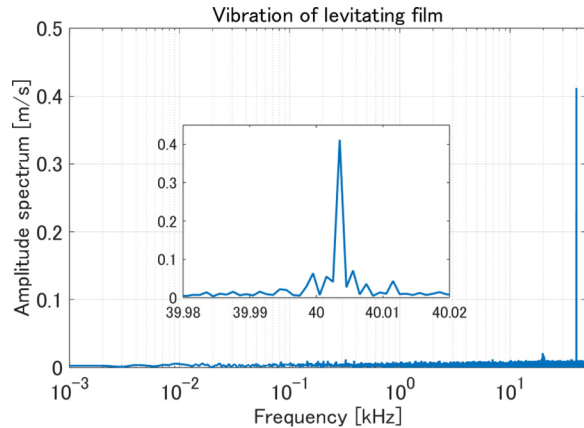


FIG. 7. Fourier transform of the measured vibration time waveform with a steep peak at 40.004 kHz.

The amplitude spectra peaked at 40.004 kHz for both films, with values of 0.86 and 0.88 m/s. Note that the peak values may vary depending on the in-plane measurement positions.

The experimental results showed that the levitation positions of the film vary with the film size and phase difference $\Delta\phi$. The levitation heights H_{film} that depend only on $\Delta\phi$ are the nodes of the standing wave acoustic pressure generated only by incident waves, as in the previous film levitation.⁶ In the xy direction, the levitation positions distribute in grid-like patterns, according to the film size. Simultaneously, the posture of the film was fixed so that the edges were parallel to the directions of the transducer alignment. **Figure 8** depicts the centers and edges of the 40- and 50-mm square films extracted from **Fig. 5**. Two pairs of edges overlap, and when they are projected onto the lower AUPA surface, they are approximately just above the transducer centers. The incident wave on the lower AUPA only exhibits local sound pressure peaks directly above the transducer centers, suggesting that all film edges must pass through this location for stable levitation. The acoustic field generated by the AUPA has a periodicity that

TABLE I. Typical physical properties of the films used in the experiment. The films with underlined thickness values were not confirmed to be levitated. For products for which representative values were not identified, values for major substances are listed in parentheses. The Young's modulus for paper is based on the measured value for Indian paper,²³ which is the closest to the tested paper in this study among previous studies.^{23–26} The out-of-plane Poisson's ratio of paper is close to zero²⁷ but was left blank because no specific value could be referenced from previous studies.^{28–30}

Film	Model No.	Density, σ/h , (mg/mm^3)	Young's modulus, E , (GPa)	Poisson's ratio, ν [-]	Thickness, h (μm)
Polyimide	TORAY, Kapton (20EN)	1.42	5	0.29–0.30	5
Polyester	TORAY, Lumirror (5-F53, 12-F68 16-F68, 19-F60, 25-S10, 38-S10)	1.4	5	0.30–0.35	5, 12, 16, 20, 25, <u>38</u>
Aramid	TORAY, Mictron (4YGE10, 12F10)	1.5	10	0.3	4.4, 12
Aluminum	Al(4N)	2.7	69	0.34	5
Titanium	TP270C	4.5	106	0.34	1, 5, <u>10</u>
Silicone rubber	TOGAWA RUBBER, K-125	1.17	1.98×10^{-3}	0.5	<u>50</u>
FEP	DAIKIN, NR0538-01	2.25	(0.35)	(0.35)	<u>25</u>
Paper	...	0.7	(MD:4.27, CD:1.45) ²³	...	30, <u>40</u>

Incident wave from the lower AUPA and levitation positions

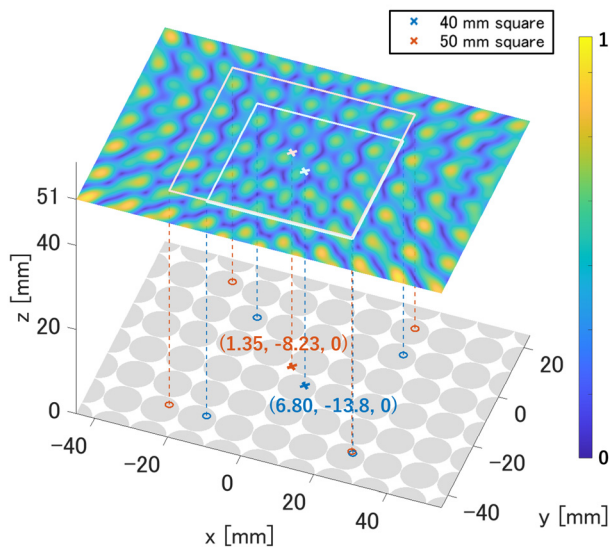


FIG. 8. A part of the distribution of the normalized acoustic pressure amplitude of the incident wave from the lower AUPA. The incident wave from the upper AUPA and re-radiation by the film are ignored. Examples of levitation positions with the condition $\Delta\phi = \pi$. The contours of the film are overlaid. The centers and vertices of the films are projected onto $z=0$ as \times and \circ , respectively.

depends on the transducer alignment. Therefore, the films had different grid-like levitation positions that depend on the lengths of the edges in each direction, rather than the center of gravity. The averages of the levitation interval in Fig. 5 were 10.5 and 10.9 mm in the x and y directions, respectively, which were close to the transducer spacing of 10.16 mm.

For other sizes, 10 N mm square polyimide films (N is an integer, $1 \leq N \leq 10$) could levitate. Larger films can levitate by arranging more AUTD3 units because the upper limit depends on the aperture of the AUPA. A smaller 5 mm square film remained stable at a specific position but occasionally rotated around the vertical axis, as reported in a previous study.⁶ Consequently, it did not satisfy the levitation criteria presented in this paper. This may be attributable to the influences of local imbalances caused by the acoustic field, which is not strictly periodic. In addition, a 45-mm square film did not levitate stably near the center of the AUPA aperture but did levitate while protruding near the outer edge of the AUPA aperture. These results are likely attributable to the incident angle tilting from vertical to horizontal at this location, which would result in a longer horizontal period of the acoustic field. In posture $\theta = 45^\circ$, films temporarily levitated without rotating but did not remain stable for more than 5 s. This posture appears to be relatively unstable and vulnerable to disturbance. In the 45° direction, the periodicity of the transducer alignment increases by a factor of $\sqrt{2}$. A 43 ($\approx 3 \times 10.16 \times \sqrt{2}$)-mm square film was tested but did not remain stable. Therefore, the initial posture should be kept close to $\theta = 0^\circ$.

We found that films did not levitate for some thicknesses and materials. The thickness h and surface density σ of each film are plotted in Fig. 9. The films are suspended in mid-air by the acoustic radiation force. The films with large surface densities cannot be levitated

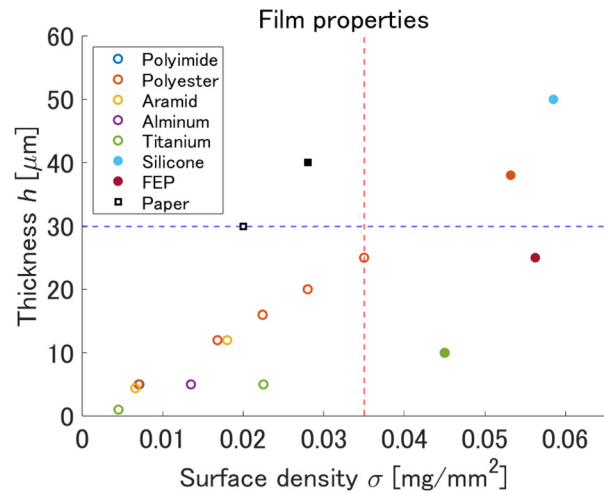


FIG. 9. Properties of the films examined, regarding whether they levitate for more than 30 s. Marks for films that could not levitate are filled in. The red line shows the maximum value of σ , and the blue line shows the maximum value of h .

because this force is an areal force. The largest surface density confirmed to levitate in this experiment was $3.5 \times 10^{-2} \text{ mg/mm}^2$ of the $25 \mu\text{m}$ polyester film. However, thicker films with a smaller surface density, such as $40 \mu\text{m}$ paper, could not levitate. These results may be attributable to larger thicknesses being less likely to vibrate at the source frequency, as shown in Fig. 7. The flexural rigidity of a flat plate is expressed as $D = \frac{Eh^3}{12(1-\nu^2)}$, where E is the Young's modulus, ν is the Poisson's ratio, and h is the thickness. The rigidity D depends on the material (E and ν) and increases with the cube of the thickness. Film vibration is expected to occur as a flexural wave whose wavelength λ_{flex} is calculated as³¹ $\lambda_{\text{flex}} = \sqrt[4]{\frac{\pi \rho \omega^2}{D}}$. The larger the rigidity, the closer the film is to a rigid plate, the less likely it is to vibrate. Thus, such films are difficult to be levitated using our method.

The films levitate when the constraining force is sufficiently larger than the disturbances. Because the constraining force depends on the acoustic pressure, films featuring higher surface density are expected to levitate with strong sound sources. Disturbances include acoustic streaming, such as Eckhardt streaming. In the standing wave without the film, the measured wind velocity was 0.15 m/s, which is sufficiently small. However, near the edge of the film, tangential flows on the front and back surfaces may merge and generate vortices.³² The effect of this phenomenon has not yet been quantified.

The remaining question is how the thin film is subjected to the horizontal constraint force. Based on the aforementioned discussion, we hypothesized that the vibrating film is subjected to a reaction force to the re-radiation of ultrasonic waves (Fig. 10). Near the edge of the film, that is, the free edge, the vibration amplitude tends to be large. Moreover, the sound wave radiation becomes asymmetric between the in-plane and out-of-plane directions here, which may cause the non-negligible out-of-plane re-radiation of ultrasonic waves at each edge. In such a case, the position of the entire film is determined by the positional relationship between the film edges and the acoustic field, as horizontal constraining forces are generated, especially near the edges. The simulation of the acoustic field on the film surface is difficult

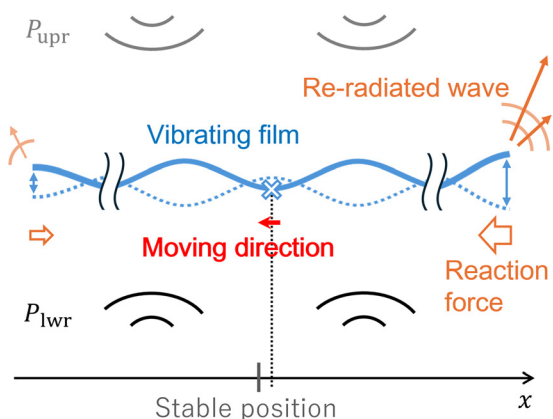


FIG. 10. Illustration of a hypothetical vibrating film levitating at a particular position. If the vibrations at both edges of the film are significantly different, then the film will move, owing to the net reaction force. Moreover, if there is a position at which this force acts as a restoring force, that position is the levitation position.

because the film thickness is too small, compared with the wavelength and surface size. Moreover, the boundary conditions are not self-evident because the film is not rigid, which is an issue for future research.

In summary, we presented a method for levitating approximately 1–25 μm thick films in the air with AUPAs vertically opposite to each other. The position measurement results showed that the films levitated at heights at which sound pressures weakened each other, and that the horizontal positions were discretely distributed at approximately each transducer interval. The levitated film vibrated at the same frequency as the ultrasonic transducer and could not be regarded as a rigid body with respect to ultrasonic waves. Moreover, sufficiently thin metal foils and polymer films also levitated using this technique. Our method enables us to hold film samples or cell samples on a film in the air and project digital images to the film as an aerial screen. Recent developments in acoustic levitation technology, such as its adaptation to underwater applications^{33,34} and the development of non-contact weighing methods,^{35–37} offer potential for a wider range of applications.

This work was supported by the Japan Society for the Promotion of Science (JSPS) KAKENHI under Grant Nos. 24KJ0554 and 21H05301.

AUTHOR DECLARATIONS

Conflict of Interest

The authors have no conflicts to disclose.

Author Contributions

Gakuto Arakawa: Conceptualization (equal); Formal analysis (lead); Funding acquisition (supporting); Methodology (lead); Writing – original draft (lead). **Shun Suzuki:** Conceptualization (equal); Software (lead); Writing – review & editing (supporting). **Takaaki Kamigaki:** Conceptualization (equal); Resources (equal); Writing – review & editing (supporting). **Yasutoshi Makino:** Conceptualization (equal); Funding acquisition (lead); Supervision (equal); Writing – review &

editing (lead). **Hiroyuki Shinoda:** Resources (equal); Supervision (equal).

DATA AVAILABILITY

The data that support the findings of this study are available from the corresponding author upon reasonable request.

REFERENCES

- ¹Ochiai, T. Hoshi, and J. Rekimoto, “Pixie dust: Graphics generated by levitated and animated objects in computational acoustic-potential field,” *ACM Trans. Graph.* **33**, 1 (2014).
- ²L. Cox, A. Croxford, B. W. Drinkwater, and A. Marzo, “Acoustic lock: Position and orientation trapping of non-spherical sub-wavelength particles in mid-air using a single-axis acoustic levitator,” *Appl. Phys. Lett.* **113**, 054101 (2018).
- ³V. Contreras and K. Volke-Sepulveda, “Enhanced standing-wave acoustic levitation using high-order transverse modes in phased array ultrasonic cavities,” *Ultrasonics* **138**, 107230 (2024).
- ⁴I. N. Ezcurdia, R. Morales, M. A. B. Andrade, and A. Marzo, “Levprint: Contactless fabrication using full acoustic trapping of elongated parts,” in *ACM SIGGRAPH 2022 Conference Proceedings, SIGGRAPH ’22* (Association for Computing Machinery, New York, NY, USA, 2022).
- ⁵H. Wu, J. Zhu, X. Wang, and Y. Li, “Design of ultrasonic standing wave levitation support for three-dimensional printed filaments,” *J. Acoust. Soc. Am.* **149**, 2848–2853 (2021).
- ⁶M. W. Kepa, T. Tomizaki, Y. Sato, D. Ozerov, H. Sekiguchi, N. Yasuda, K. Aoyama, P. Skopintsev, J. Standfuss, R. Cheng, M. Hennig, and S. Tsujino, “Acoustic levitation and rotation of thin films and their application for room temperature protein crystallography,” *Sci. Rep.* **12**, 5349 (2022).
- ⁷D. E. Lucchetta, P. Castellini, M. Martarelli, L. Scalise, G. Pandarese, C. Riminesi, G. Singh, A. Di Donato, O. Francescangeli, and R. Castagna, “Light-controlled rotational speed of an acoustically levitating photomobile polymer film,” *Materials* **16**, 553 (2023).
- ⁸S. Inoue, S. Mogami, T. Ichiyama, A. Noda, Y. Makino, and H. Shinoda, “Acoustical boundary hologram for macroscopic rigid-body levitation,” *J. Acoust. Soc. Am.* **145**, 328–337 (2019).
- ⁹A. Marzo, S. A. Seah, B. W. Drinkwater, D. R. Sahoo, B. Long, and S. Subramanian, “Holographic acoustic elements for manipulation of levitated objects,” *Nat. Commun.* **6**, 8661 (2015).
- ¹⁰S. Zehnter, M. A. B. Andrade, and C. Ament, “Acoustic levitation of a Mie sphere using a 2D transducer array,” *J. Appl. Phys.* **129**, 134901 (2021).
- ¹¹A. L. Yarin, M. Pfaffenlehner, and C. Tropea, “On the acoustic levitation of droplets,” *J. Fluid Mech.* **356**, 65–91 (1998).
- ¹²D. Zang, K. Lin, L. Li, Z. Chen, X. Li, and X. Geng, “Acoustic levitation of soap bubbles in air: Beyond the half-wavelength limit of sound,” *Appl. Phys. Lett.* **110**, 121602 (2017).
- ¹³S. Santesson and S. Nilsson, “Airborne chemistry: Acoustic levitation in chemical analysis,” *Anal. Bioanal. Chem.* **378**, 1704–1709 (2004).
- ¹⁴B. W. Drinkwater, “A perspective on acoustical tweezers—devices, forces, and biomedical applications,” *Appl. Phys. Lett.* **117**, 180501 (2020).
- ¹⁵I. I. I. Al-Nuaimi, M. N. Mahyuddin, and N. K. Bachache, “A non-contact manipulation for robotic applications: A review on acoustic levitation,” *IEEE Access* **10**, 120823–120837 (2022).
- ¹⁶L. Gao, P. Irani, S. Subramanian, G. Prabhakar, D. Martinez Plasencia, and R. Hirayama, “Datalev: Mid-air data physicalisation using acoustic levitation,” in *Proceedings of the 2023 CHI Conference on Human Factors in Computing Systems, CHI ’23* (Association for Computing Machinery, New York, NY, USA, 2023).
- ¹⁷R. Hirayama, G. Christopoulos, D. M. Plasencia, and S. Subramanian, “High-speed acoustic holography with arbitrary scattering objects,” *Sci. Adv.* **8**, eabn7614 (2022).
- ¹⁸H. Bruus, “Acoustofluidics 7: The acoustic radiation force on small particles,” *Lab Chip* **12**, 1014–1021 (2012).

- ¹⁹T. Tang and L. Huang, "An efficient semi-analytical procedure to calculate acoustic radiation force and torque for axisymmetric irregular bodies," *J. Sound Vib.* **532**, 117012 (2022).
- ²⁰M. A. B. Andrade, F. T. A. Okina, A. L. Bernassau, and J. C. Adamowski, "Acoustic levitation of an object larger than the acoustic wavelength," *J. Acoust. Soc. Am.* **141**, 4148–4154 (2017).
- ²¹S. Tsujino, Y. Sato, S. Jia, M. W. Kepa, S. Trampari, and T. Tomizaki, "Inertial mixing of acoustically levitated droplets for time-lapse protein crystallography," *Droplet* **3**, e132 (2024).
- ²²S. Suzuki, S. Inoue, M. Fujiwara, Y. Makino, and H. Shinoda, "Autd3: Scalable airborne ultrasound tactile display," *IEEE Trans. Haptics* **14**, 740–749 (2021).
- ²³M. Horie and S. Onogi, "Dynamic measurements of physical properties of pulp and paper by audiofrequency sound," *J. Appl. Phys.* **22**, 971–977 (1951).
- ²⁴K. Mazen, T. G. Eymin, and S. André, "Contactless measurement of the elastic young's modulus of paper by an ultrasonic technique," *Ultrasonics* **37**, 133–139 (1999).
- ²⁵E. T. Filipov, K. Liu, T. Tachi, M. Schenk, and G. H. Paulino, "Bar and hinge models for scalable analysis of origami," *Int. J. Solids Struct.* **124**, 26–45 (2017).
- ²⁶G. Morgan, K. Gustav, M. Axel, F. Mats, W. Kenneth, and E. Fredrik, "Network model for predicting structural properties of paper," *Nord. Pulp Pap. Res. J.* **37**, 712–724 (2022).
- ²⁷N. Stenberg and C. Fellers, "Out-of-plane Poisson's ratios of paper and paper-board," *Nord. Pulp Pap. Res. J.* **17**, 387–394 (2002).
- ²⁸K. Schulgasser, "The in-plane Poisson ratio of paper," *Fibre Sci. Technol.* **19**, 297–309 (1983).
- ²⁹L. Götschling and H. Baumgarten, "Triaxial deformation of paper under tensile load," in *Fundamental Properties Paper Related to Its Uses*, edited by F. Bolam (NC State University, 1976), Vol. 1, pp. 227–252.
- ³⁰S. Włodzimierz, "Determination of Poisson's ratio in the plane of the paper," *Fibres Text. East. Eur.* **16**, 117–120 (2008).
- ³¹A. Darabi, A. Zareei, M.-R. Alam, and M. J. Leamy, "Broadband bending of flexural waves: Acoustic shapes and patterns," *Sci. Rep.* **8**, 11219 (2018).
- ³²B.-G. Loh, S. Hyun, P. I. Ro, and C. Kleinstreuer, "Acoustic streaming induced by ultrasonic flexural vibrations and associated enhancement of convective heat transfer," *J. Acoust. Soc. Am.* **111**, 875–883 (2002).
- ³³Y.-R. Jia, D.-J. Wu, J. Yao, Q. Wei, Z. Xu, and X.-J. Liu, "Acoustic tweezing for both Rayleigh and Mie particles based on acoustic focused petal beams," *Appl. Phys. Lett.* **116**, 263504 (2020).
- ³⁴Y. Yang, T. Ma, Q. Zhang, J. Huang, Q. Hu, Y. Li, C. Wang, and H. Zheng, "3d acoustic manipulation of living cells and organisms based on 2d array," *IEEE Trans. Biomed. Eng.* **69**, 2342–2352 (2022).
- ³⁵J. Nakahara and J. R. Smith, "Acoustic balance: Weighing in ultrasonic non-contact manipulators," *IEEE Robot. Autom. Lett.* **7**, 9145–9150 (2022).
- ³⁶Y. Wang, L. Jiang, Z. Chen, H. Zhang, and X. Li, "Contactless weighing method based on deep learning and acoustic levitation," *Meas. Sci. Technol.* **35**, 056005 (2024).
- ³⁷M. Morrell and D. G. Grier, "Acoustodynamic mass determination: Accounting for inertial effects in acoustic levitation of granular materials," *Phys. Rev. E* **108**, 064903 (2023).